University of Sistan and Baluchestan

Chemical Process Design

Available online at http://cpd.usb.ac.ir/

CFD Analysis of VX Gas Dispersion in an Indoor Environment

Hassan Tavakoli[1]✉, Rasool Amirkhani[2]

[1] Chemistry Group, Faculty of Basic Sciences, Imam Ali University, Iran. E-mail: hs.tavakoli51@gmail.com
[2] Chemistry Group, Faculty of Basic Sciences, Imam Ali University, Iran. E-mail: amirkhani_rasool@yahoo.com

ARTICLE INFO

Article type:
Research Article

Article history:
Received: 2025-01-26
Received in revised form: 2025-04-15
Accepted: 2025-04-21
Published online: 2025-04-21

Keywords: *Nerves Gas Dispersion; Indoor Environment; CFD*

ABSTRACT

VX, a highly persistent and lethal nerve agent, presents a severe threat in enclosed spaces during chemical attacks or accidental releases. However, its dispersion behavior within indoor environments remains poorly understood, limiting the effectiveness of mitigation and response strategies. This study introduces the first transient three-dimensional computational fluid dynamics (CFD) analysis of VX gas dispersion and removal in a confined space, defining novel safety metrics: danger time (time to reach a toxic 10 mg/m³) and safe time (time to decline below a safe 0.1 mg/m³). Employing the k-epsilon turbulence model in COMSOL Multiphysics, we investigated the effects of air inlet velocity (0.5–1.5 m/s), inflow VX concentration (100–300 mg/m³), and initial VX concentration (500–1000 mg/m³) in a validated room-scale model. Results reveal that elevating inlet velocity from 0.5 to 1.5 m/s reduces safe time by 67.1% (40.8 to 13.4 min), enhancing decontamination, while increasing inflow concentration from 100 to 300 mg/m³ accelerates danger time by 70% (0.2 to 0.06 min), and amplifying risk onset. Higher initial concentrations extend safe time by 9.3%, reflecting slower dilution. VX accumulates near walls, driven by mixing effects, identifying critical hazard zones. Moreover, the results show that incorporating obstacles into the indoor environment increases both the danger and the required safety times.

Cite this article: Tavakoli, H., Amirkhani, R., (2025), CFD Analysis of VX Gas Dispersion in an Indoor Environment, *Chemical Process Design*, 4(1), 60-73. http//doi.org/10.22111/cpd.2025.50928.1047

DOI: http//doi.org/10.22111/cpd.2025.50928.1047

Publisher: University of Sistan and Baluchestan.

1. Introduction

Chemical warfare agents (CWAs) have been stockpiled in significant quantities across various regions due to their historical use in military operations [1]. Their continued presence poses serious environmental and security risks, particularly in remote or hard-to-access areas where containment is more difficult [2]. As such, the rapid and safe

destruction of CWAs has become a critical global priority. International protocols emphasize the urgency of neutralizing these agents to prevent accidental release or deliberate misuse [4]. Moreover, effective disposal not only protects ecosystems but also supports compliance with international disarmament agreements [5].

The global threat posed by chemical warfare agents such as VX and sarin has driven significant progress in detection technologies, elimination of stockpiles, and development of effective decontamination strategies [6]. Protecting both military personnel and civilian populations remains the central objective of these efforts [7]. A crucial aspect of countering the effects of sarin involves understanding its interaction with different surfaces, as surface chemistry influences persistence and removal methods [8]. Due to the extreme toxicity of sarin, researchers often rely on simulants or less hazardous substances to study its behavior under controlled conditions [9, 10].

Chauhan et al. [11] examined gas distribution indoors using CFD modeling in a naturally ventilated living room. This study aimed to evaluate activity levels and the effects of natural ventilation on indoor radon concentrations. The results of the simulations were consistent with the measured data. Zhuo et al. [12] also employed CFD to analyze the three-dimensional distribution of hazardous gases, revealing that gas distribution in a naturally ventilated room was generally uniform, except in areas near the air inlets. Hossaini et al. [13] used CFD to model the dispersion of sarin gas in a subway station, comparing scenarios with and without a train. Their results indicated that, without a train, sarin concentrations reached lethal levels (8.9mg/m^3) within 20 minutes. However, the train's piston effect significantly reduced the sarin concentration to 25 mg/m^3, underscoring the importance of ventilation and rapid response in mitigating this threat.

Parkash et al. [14] conducted an investigation into the application of CFD in the analysis of indoor environments, providing a comprehensive review of prevalent CFD models utilized for gas dispersion. They underscored the significance of CFD in the assessment of indoor hazards and identified various areas necessitating further research. Faugier et al. [15] employed CFD to develop numerical models of existing subway stations, incorporating several simplifying assumptions. The objective of their study was to forecast the impact of train-induced wind on airflow patterns; however, the inherent complexity of airflow sources restricted the broader applicability of their findings. Furthermore, they supplied a detailed comparison between their numerical predictions and field tests conducted within an actual subway station setting.

Lin et al. [16] utilized a CFD-based back propagation neural network (BPNN) to examine pollutant dispersion in an urban context. Their findings revealed that ambient airflow separated from reversed flow in the leeward zones of buildings, which impeded the removal of pollutants. Nonetheless, they found that reducing gas emissions effectively mitigated the presence of hazardous pollutants. Yang et al. [17] applied CFD simulations to assess wind velocity, temperature, and air age distribution within a bedroom equipped with a wall-mounted air conditioning system during the summer months. The results indicated that the system effectively managed indoor thermal loads, ensuring satisfactory thermal comfort, with moderate air velocities in occupied areas that adhered to summer wind comfort standards.

Widiatmojo et al. [18] implemented CFD to model gas dispersion within a subway station, utilizing discretized mass transfer principles based on Brownian motion. Their model was validated through tracer gas dispersion experiments, demonstrating reasonable accuracy. Dolezal et al. [19] utilized AnyLogic software to develop an agent-based model simulating a portion of the 1995 Tokyo subway sarin gas attack. By exploring various hypothetical scenarios, they sought to identify strategies aimed at minimizing losses and casualties in comparable terrorist events. Siddiqui et al.

[20] examined the environmental hazards associated with the release of dense hazardous chemicals in indoor industrial settings. They created a CFD-based model to evaluate the risks of an accidental, extended, and undetected chlorine gas leak. Their simulations indicated that the dense chlorine gas behaves akin to a liquid, spreading along the floor and progressively increasing in concentration with height, thus demonstrating both stratification and dilution effects. Xu et al. [21] conducted a CFD-based simulation to investigate indoor gas leakage dispersion under various conditions, including ventilation, gas type, and leakage rate. The results highlight key safety implications and offer an effective educational tool for enhancing engineering students' CFD skills and risk awareness. Li et al. [22] investigated the Ceiling-Fan-Integrated-Air Conditioning (CFIAC) system using both experimental and CFD methods to assess airflow, and air quality. Their findings reveal that operating the ceiling fan at Level 4 downward significantly improves ventilation, reduces CO_2 concentrations, and lowers the risk of cross-infection, offering an efficient cooling solution with health benefits. Wang et al. [23] developed a CFD-based 3D gas dispersion model coupled with the iterative ensemble Kalman filter to estimate heavy gas leakage parameters and concentration distribution. Applied to H_2S leakage, the approach significantly improved prediction accuracy and efficiency, offering a reliable method for safety assessment in enclosed workplaces.

Previous studies have investigated the dispersion of nerve gases through CFD models. However, there is a pressing need to explore the dispersion of VX gas in indoor environments, particularly to establish the safe and danger times associated with its presence. The "danger time" indicates the interval during which VX gas concentration reaches 10 mg/m^3 indoors, posing significant health risks, including potentially fatal outcomes. Conversely, the "safe time" signifies the duration during which the concentration of VX gas falls below 0.1 mg/m^3 due to the influx of fresh air. Analyzing these factors across two distinct scenarios is crucial for enhancing safety measures and the design of indoor environments.

This study investigates the dispersion of VX gas in an indoor environment using a three-dimensional CFD model. The model is first verified and validated to ensure accuracy. Subsequently, the velocity distribution and concentration profiles of VX gas are analyzed. To calculate danger time, the initial VX gas concentration in the indoor environment is zero, and the gas enters with the air. In contrast, for calculating safe time, the initial VX gas concentration in the indoor environment is not zero, but the incoming air is fresh and free of VX gas. This analysis enhances our understanding of VX gas behavior indoors and provides valuable insights for improving emergency response strategies.

2. Method

This study examines the dispersion of VX gas in an indoor environment by employing a transient three-dimensional CFD model. The CFD model utilizes the equations of continuity, momentum, and mass transfer, in conjunction with the k-epsilon turbulence model using standard wall functions. This modeling approach enables the simulation of fluid flow and mass transfer within the indoor setting. The model is designed to quantify the time at which the concentration of VX gas reaches 10 mg/m^3, identified as the threshold for danger, as well as the time required for the concentration to decrease to 0.1 mg/m^3, which signifies a return to safe levels.

The indoor environment under investigation is characterized as a typical room with an air inlet and an open area, such as the space beneath a door. Figs. 1(a), 1(b), 1(c), and 1(d) illustrate the three-dimensional indoor environment, the

outlet area, the inlet air region, and critical corners of the indoor space where the concentration of VX gas was calculated.

2.1. Governing equations and boundary conditions

The CFD model simulates VX gas dispersion using a transient three-dimensional approach, incorporating equations for continuity, momentum, turbulence (k-epsilon with standard wall functions), and mass transfer (Equations 1–8). To ensure computational tractability and focus on key dispersion mechanisms, several assumptions are employed. First, the flow is assumed to be three-dimensional, turbulent, and unsteady, capturing the complex, chaotic air movement typical of indoor environments with natural or mechanical ventilation [24].

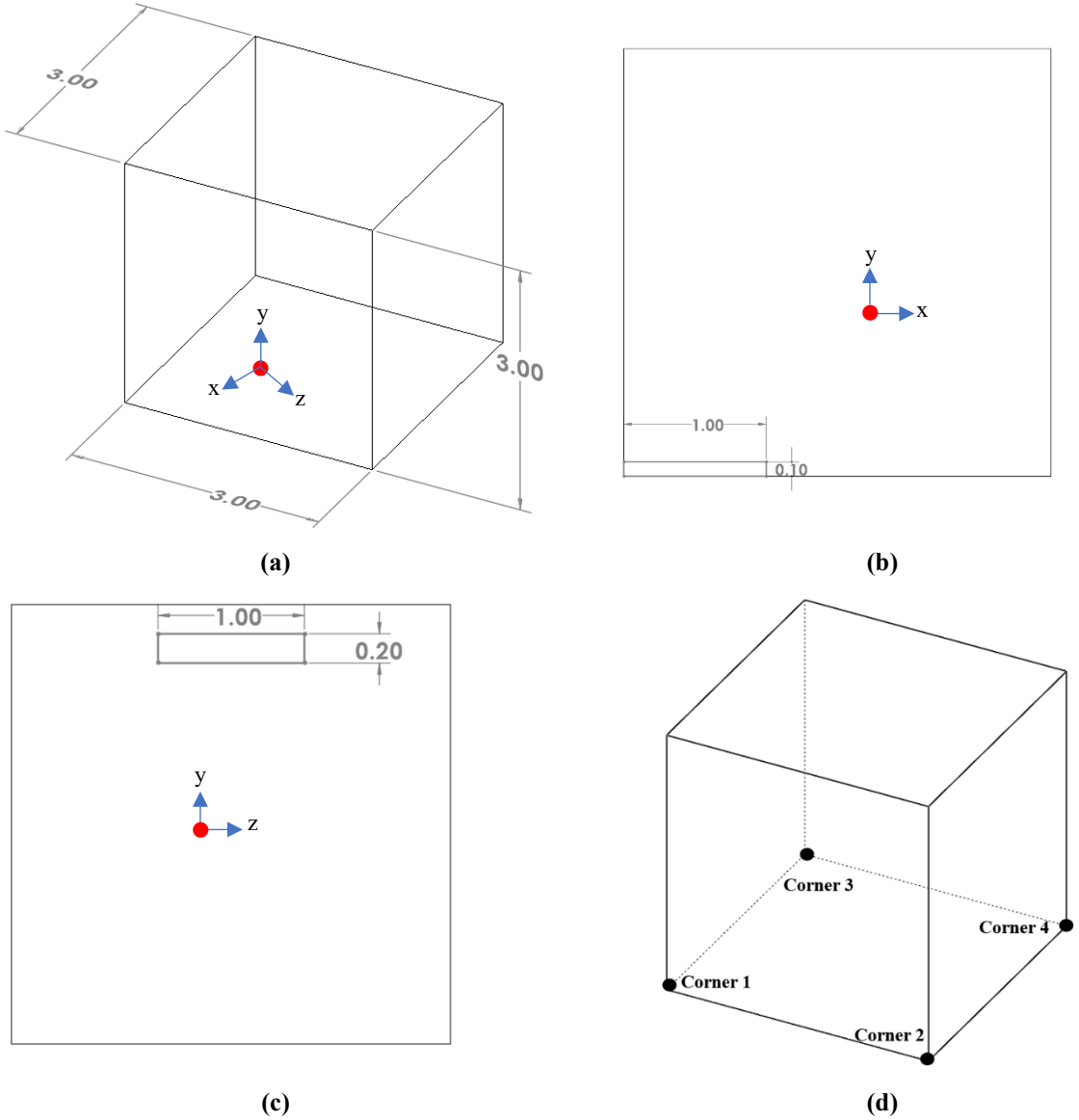

Fig. 1. (a) Three-dimensional indoor environment; (b) the outlet region; (c) the inlet air region; (d) the essential corners of the indoor environment; All dimensions are in meters

This reflects realistic conditions where VX dispersion is driven by convective mixing rather than laminar flow. Second, the system is treated as isothermal at 25°C, neglecting temperature gradients. This assumption simplifies the model by excluding heat transfer effects, justified by VX's low volatility (vapor pressure ~0.0007 mmHg at 25°C), which limits vaporization-driven variations under standard indoor conditions. While temperature fluctuations could

influence air density or diffusion in extreme scenarios, their impact is minimal here given the study's focus on short-term dispersion. Third, boundary conditions include a no-slip condition at walls, atmospheric pressure at the outlet, and specified velocity and concentration at the inlet (Table 1), approximating a typical room with a single air entry and exit (such as a door gap). For danger time calculations, the initial VX concentration is zero indoors, with contaminated air entering; for safe time, the initial concentration is non-zero, with fresh air introduced. These assumptions align the model with a controlled yet representative indoor setting, balancing accuracy and practicality. Equations are solved using COMSOL Multiphysics via the finite element method. Based on these conditions, the governing equations for continuity, momentum, turbulence, and mass transfer can be expressed as follows [25-27]:

Continuity
$$\rho\frac{\partial \mathbf{u}}{\partial t}+\rho\nabla.\mathbf{u}=0 \tag{1}$$

Momentum
$$\rho\frac{\partial \mathbf{u}}{\partial t}+\rho(\nabla.\mathbf{u})\mathbf{u}=\nabla.[-pI+K] \tag{2}$$
$$K=\mu(\nabla\mathbf{u}+(\nabla\mathbf{u})^{T})$$

Kinetic energy:
$$\rho(\mathbf{u}.\nabla)k=\nabla.\left[\left(\frac{\mu_T}{\sigma_k}+\mu\right)\nabla k\right]+P_k-\rho\varepsilon \tag{3}$$

Dispersion
$$\rho(\mathbf{u}.\nabla)\varepsilon=\nabla.\left[\left(\frac{\mu_T}{\sigma_k}+\mu\right)\nabla\varepsilon\right]+\frac{C_{\varepsilon 1}\varepsilon}{k}P_k-\frac{C_{\varepsilon 2}\rho\varepsilon^2}{k} \tag{4}$$

Turbulent term
$$P_k=\mu_T[\,\nabla\mathbf{u}:(\nabla\mathbf{u}+(\nabla\mathbf{u})^{T})-\frac{2}{3}(\nabla\mathbf{u})^2]-\frac{2}{3}\rho k\nabla.\mathbf{u}] \tag{5}$$

Turbulent viscosity
$$\mu_T=\frac{\rho C_\mu k^2}{\varepsilon} \tag{6}$$

Mass transfer
$$\frac{\partial c}{\partial t}+\nabla.(-D\nabla c)+\mathbf{u}.\nabla c=0 \tag{7}$$

Diffusion coefficient
$$D=\frac{4.14\times10^{-4}T^{1.9}\sqrt{\frac{1}{MW_B}+\frac{1}{MW_A}}MW_A^{-0.33}}{p} \tag{8}$$

In these equations, u represents the velocity vector, ρ is the fluid density, p stands for pressure and μ denotes viscosity. The variable c refers to the concentration of the nerve agent, while D is the diffusion coefficient of gas A into air and MW represents the molecular weight. k represents the turbulent kinetic energy, and ε is the dissipation rate of turbulent kinetic energy. μ_T corresponds to the turbulent viscosity, T indicates the temperature, and $C_{1\varepsilon}$, $C_{2\varepsilon}$, and C_μ are constants used in turbulence modeling.

The boundary conditions for the model vary depending on the scenario being analyzed. For the danger time calculation, the velocity of the airflow is specified at the inlet for fluid flow, while the concentration of VX gas is defined for mass transfer. At the outlet, atmospheric pressure is applied for fluid flow, and a zero-gradient flux condition is used for mass transfer. Other boundaries are set with a no-slip condition for fluid flow and a no-flux condition for mass transfer. In this scenario, the initial concentration of VX gas in the indoor environment is set to zero.

For the safe time calculation, the velocity of the airflow is also specified at the inlet for fluid flow, but the inlet concentration of VX gas is set to zero for mass transfer. At the outlet, atmospheric pressure is applied for fluid flow,

and a zero-gradient flux condition is used for mass transfer. In this case, the initial VX gas concentration in the indoor environment is not zero. Similarly, other boundaries are assigned a no-slip condition for fluid flow and a no-flux condition for mass transfer. All equations are solved using COMSOL Multiphysics, utilizing the finite element method.

In this study, the air inlet velocity, inlet concentration of VX gas, and initial concentration of VX gas are considered input variables influencing the safe time and danger time. The range of each factor is detailed in Table 1. In this study, air inlet velocity, inlet VX gas concentration, and initial VX gas concentration are key variables affecting danger and safe times, with ranges specified in Table 1. The air inlet velocity range (0.5–1.5 m/s) reflects typical indoor ventilation rates, as established by Agarwal et al. [28] for naturally ventilated spaces, ensuring relevance to common building conditions. The inlet VX concentration (100–300 mg/m³) is based on a hypothetical release scenario informed by VX's lethal inhalation dose, spanning moderate to severe exposure levels plausible in chemical incidents. The initial VX concentration (500–1000 mg/m³) simulates a heavily contaminated indoor environment prior to ventilation, consistent with VX's low volatility and persistence, testing the limits of decontamination under extreme conditions. These ranges provide a robust framework for evaluating VX dispersion and mitigation strategies.

Table 1. Range of each factor

Factor	Range
Air inlet velocity	0.5-1.5 (m/s)
Inlet concentration of the VX gas*	100-300 (mg/m^3)
Initial value of the VX gas**	500-1000 (mg/m^3)

3. Results

3.1. Mesh independency

Fig. 2(a) and Fig. 2(b) illustrate the structured mesh of the indoor environment and demonstrate the mesh independence of the CFD model, respectively. For the mesh independence test, the inlet gas velocity was set at 1 m/s, and the inlet concentration of VX gas was 200 mg/m³. Fig. 2(b) displays the average concentration of VX gas across three different mesh configurations consisting of 80,000, 160,000, and 320,000 elements. The relative error between mesh 2 (160,000 elements) and mesh 3 (320,000 elements) is less than 0.2%. Therefore, mesh 2 is chosen as the optimized mesh for the calculations.

Fig. 2(c) presents the effect of the time step on the average concentration of VX gas. The results indicate that the relative error in average concentration between time steps of 0.1 minutes and 0.01 minutes is negligible. Consequently, a time step of 0.1 minutes is selected as the optimized value.

3.2. Model validation

This study uses data from Chauhan et al. [11] for model validation, where the distribution of gas in an indoor environment was investigated. Fig. 3 compares the results of the CFD model with the data from Chauhan et al. [11] at four locations: corners 1, 2, 3, and the center, all measured at a height of 1.22 m from the floor. The comparison shows that the average relative error between the current model and Chauhan et al.'s data is 3.3%, demonstrating strong agreement between the results.

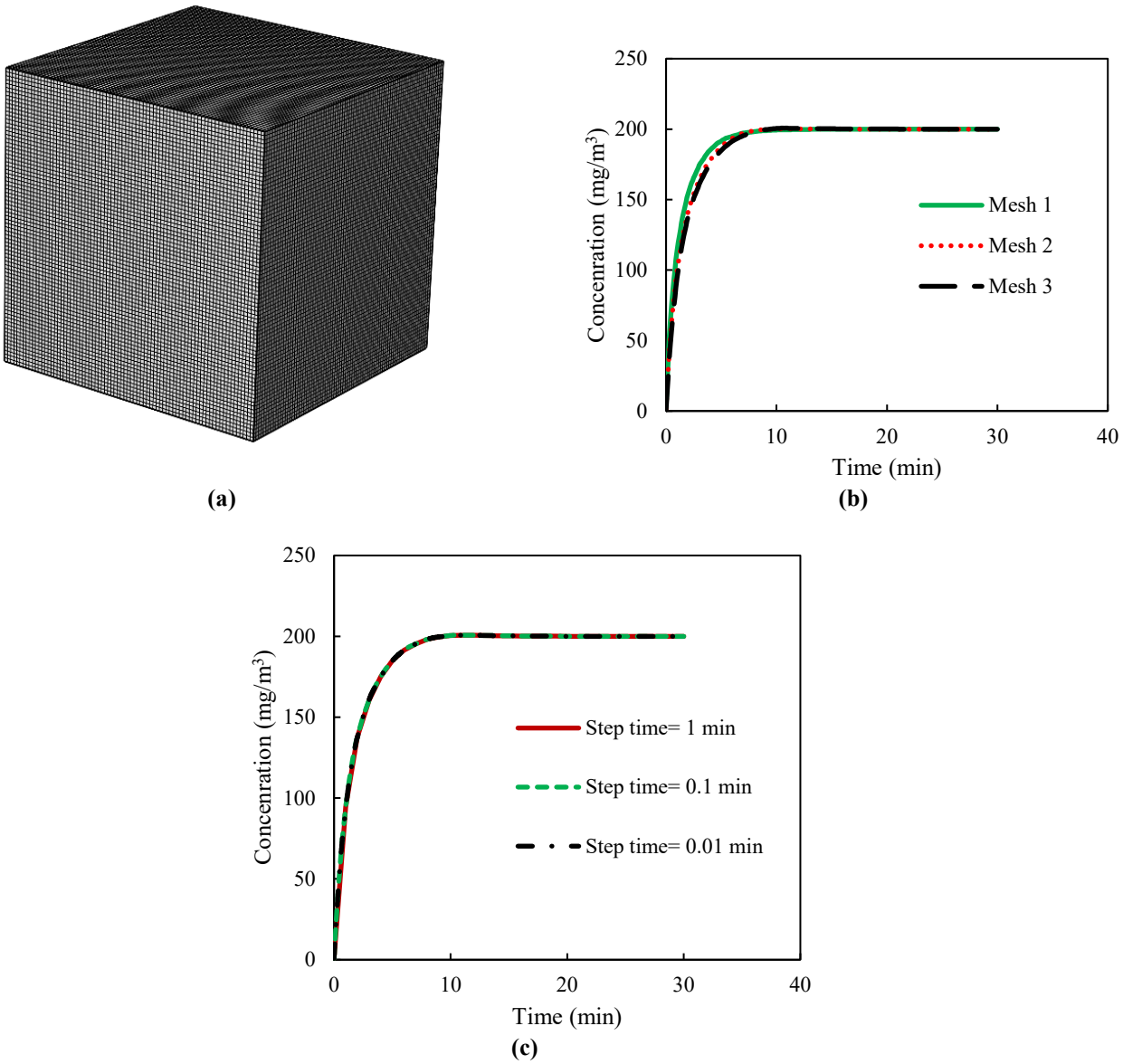

Fig. 2. (a) The mesh of domain; (b) mesh independency; (c) time step independency

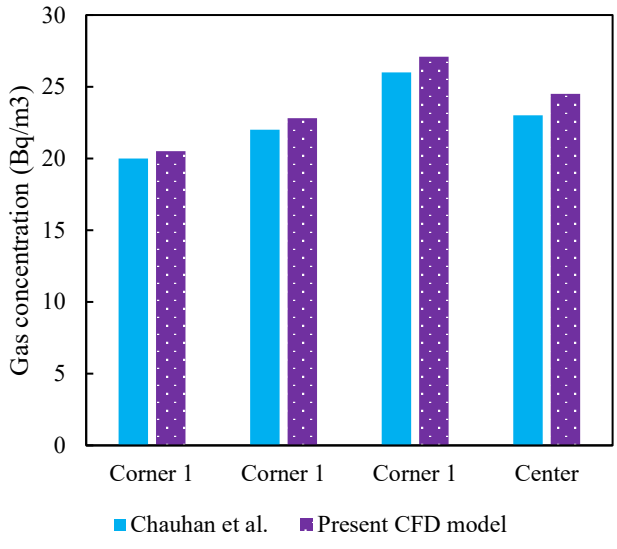

Fig. 3. Validation of the CFD model using data from Chauhan et al. [11]

3.3. Velocity and concentration distribution

Figs. 4(a), 4(b), and 4(c) illustrate the velocity distribution in the indoor environment at z = 0 m, z = 1.5 m, and z = 1.98 m, respectively, at steady state, with an inlet air velocity of 0.5 m/s and VX concentration of 100 mg/m³. The velocity in the outlet region (z = 0 m) is higher due to the reduced cross-sectional area, accelerating airflow as it exits. At mid-height (z = 1.5 m), corner regions exhibit higher velocities than the center, a result of airflow interacting with walls upon entry (z = 1.98 m). This interaction generates turbulence, acting as a mixer and creating a disturbed velocity field near corners, as evident in Fig. 4(c).

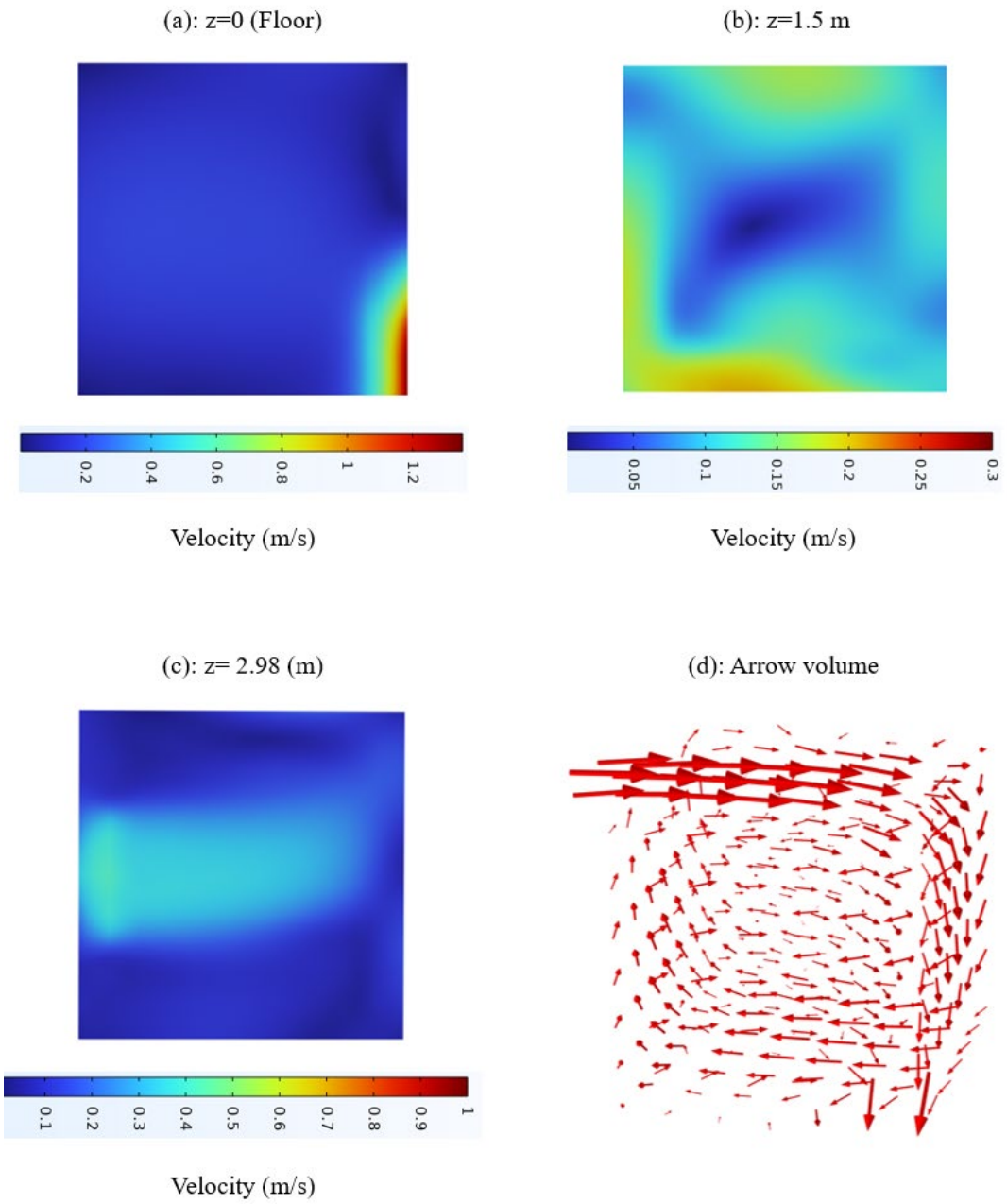

Fig. 4. Velocity distribution in the indoor environment at (a) z = 0 m; (b) z = 1.5 m; (c) z = 1.98 m; (d) Arrow volume

Fig. 5 shows the VX concentration distribution at z = 1.5 m at t = 0 min and t = 15 min. Initially zero, the concentration rises after 15 minutes, with higher values near corners than at the center. This pattern arises from two physical mechanisms: reduced air velocity near walls (due to the no-slip boundary condition) limits convective removal of VX, allowing accumulation, while wall-induced turbulence enhances local mixing, concentrating the gas in these regions. Figs. 6(a) and 6(b) detail this further, showing earlier steady-state times in corners 1 and 2 (closer to the

inlet) than 3 and 4 (near the outlet), reflecting velocity gradients. With an inflow of 100 mg/m³, the average concentration stabilizes at 100 mg/m³ after approximately 20 minutes, underscoring the role of ventilation dynamics in dispersion.

3.4. Impact of inlet velocity and inlet VX concentration on danger time

Fig. 7(a) illustrates the relationship between danger time and air inlet velocities for a VX gas concentration of 100 mg/m³. As the air inlet velocity increases, the danger time decreases. This behavior can be attributed to the enhanced convective mass transfer, which allows a greater amount of VX gas to enter the room more rapidly. Specifically, when the inlet velocity rises from 0.5 m/s to 1.5 m/s, the danger time decreases significantly, from 0.4 minutes to 0.13 minutes, representing a reduction of 67.5%. This finding highlights the critical role of air velocity in influencing the spread and impact of hazardous gases in confined spaces.

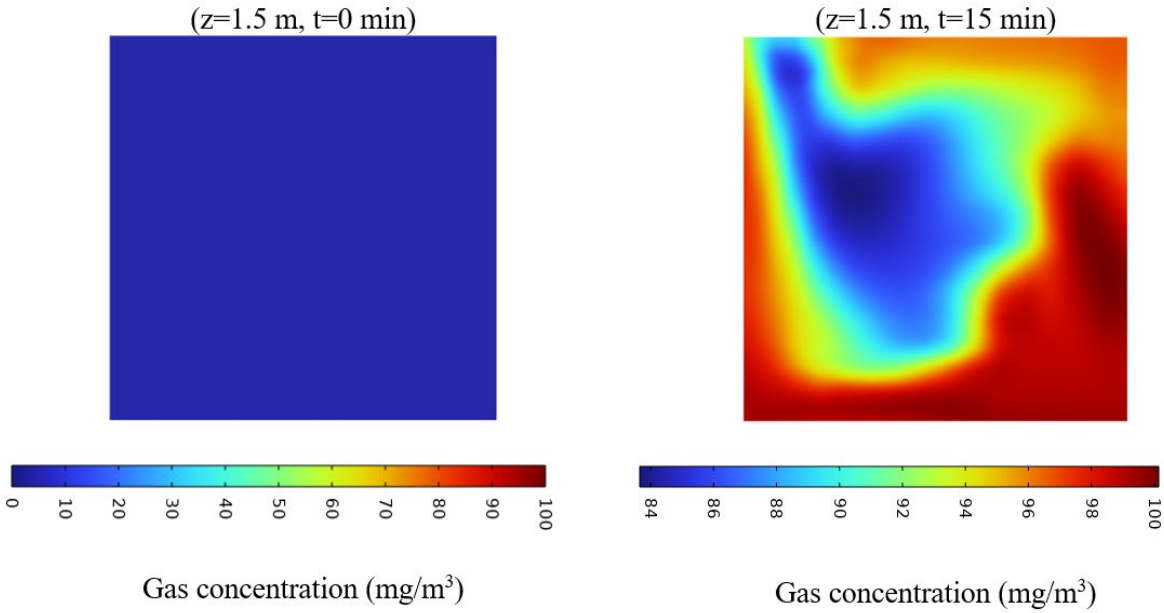

Fig. 5. VX gas concentration distribution in the indoor environment at z = 1.5 m at different times

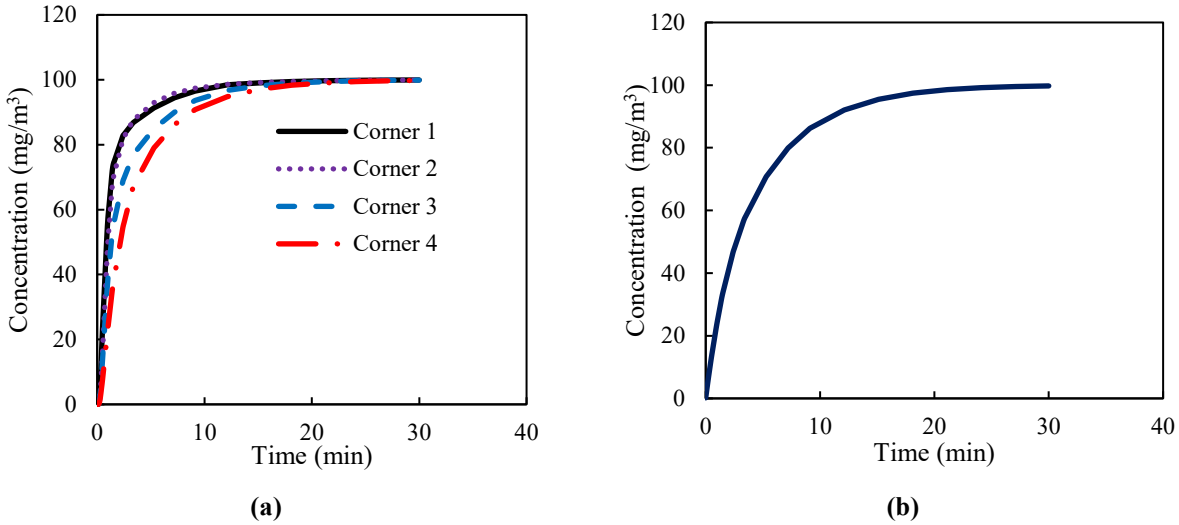

Fig. 6. Gas concentration distribution in the indoor environment at z = 1.5 m for the (a) four corners; (b) the average

Fig. 7(b) illustrates the effect of inflow concentration of VX gas on the danger time, with a fixed inlet velocity of 1 m/s. The inflow concentration of VX gas varies from 100 mg/m³ to 300 mg/m³. As the inflow concentration increases from 100 mg/m³ to 300 mg/m³, the danger time decreases from 0.2 minutes to 0.06 minutes, representing a reduction of 70%. This decrease occurs because higher inflow concentrations cause the VX gas concentration to reach the critical threshold of 10 mg/m³ more quickly in the indoor environment. The elevated inflow concentration accelerates the accumulation of VX gas in the room, thereby shortening the danger time significantly. This observation underscores the importance of inflow concentration as a critical factor influencing gas dispersion and associated risks in confined spaces.

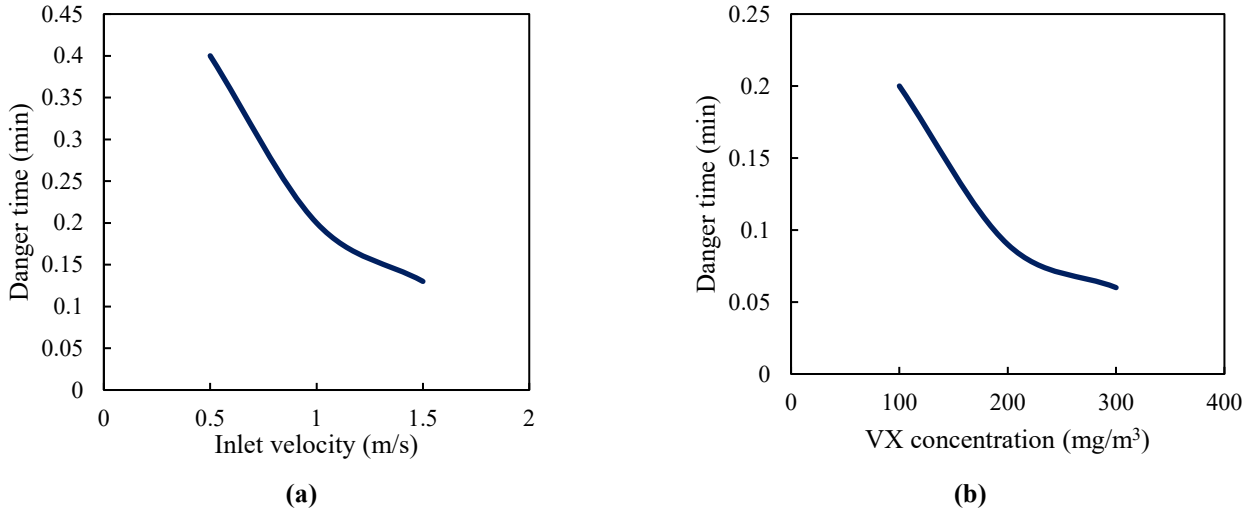

Fig. 7. Effect of inlet velocity (a) and inflow VX gas concentration (b) on danger time

3.5. Impact of inlet velocity and initial concentration on safe time

Fig. 8(a) illustrates the effect of inlet velocity on safe time at an inflow VX gas concentration of 750mg/m³. In the safe scenario, as the inlet velocity of fresh air increases, the VX gas is removed more rapidly from the indoor environment due to enhanced convective mass transfer. Specifically, when the inlet velocity increases from 0.5m/s to 1.5m/s, the safe time decreases from 40.8 minutes to 13.4 minutes, representing a reduction of 67.1%. This highlights the significant influence of inlet velocity on the rate of gas removal and the overall safety of the indoor environment.

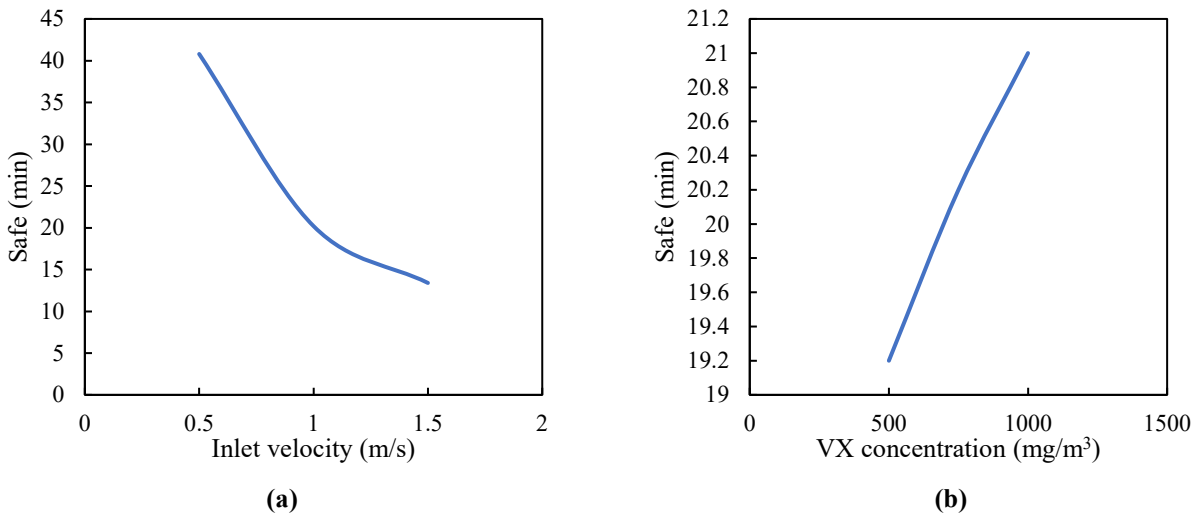

Fig. 8. Effect of inlet velocity (a) and initial VX gas concentration (b) on safe time

Fig. 8(b) illustrates the effect of the initial VX gas concentration on safe time at a fixed inlet velocity of 1 m/s. As the initial VX concentration increases, the safe time also increases. This occurs because a higher initial concentration requires more time for the VX gas concentration to decrease to below 0.1 mg/m³. Specifically, when the initial concentration increases from 500mg/m³ to 1000mg/m³, the safe time increases by 9.3%. This demonstrates that higher initial concentrations result in prolonged safe times due to the extended removal process.

The results of this CFD study on VX gas dispersion indoors reveal critical dynamics with significant implications for safety in chemical threat scenarios. The velocity and concentration distributions show VX accumulating near walls, with concentrations higher in corner regions than the center (steady-state 100 mg/m³ at 20 minutes with 100 mg/m³ inflow). This pattern, driven by wall-induced mixing, suggests that occupants near walls face elevated exposure risks, interpreting these areas as primary hazard zones where sensors or evacuation priorities should be focused.

The parametric analysis further elucidates VX's behavior. Danger times of 0.06–0.4 minutes (inflow concentration 100–300 mg/m³, velocity 0.5–1.5 m/s) indicate an alarmingly rapid onset of toxic levels (10 mg/m³), exceeding VX's lethal threshold (10–50 mg.min/m³) within seconds to minutes. This interprets as an urgent need for immediate evacuation or protective measures upon release detection, leaving little margin for delay. Conversely, safe times of 13.4–40.8 minutes (initial concentration 500–1000 mg/m³, velocity 0.5–1.5 m/s) to reach 0.1 mg/m³ reflect VX's persistence due to its low volatility (~0.0007 mmHg), suggesting that natural or moderate ventilation (0.5 m/s) is insufficient for rapid decontamination. Increasing velocity to 1.5 m/s reduces safe time by 67.1%, interpreting this as a strong case for high-capacity ventilation systems in contaminated spaces. Higher initial concentrations (1000 vs. 500 mg/m³) extending safe time by 9.3% further imply that severe releases prolong recovery, necessitating prolonged isolation or advanced air purification.

Collectively, these findings interpret VX as a uniquely persistent indoor threat, contrasting with more volatile agents, and underscore the need for tailored emergency responses—rapid evacuation for danger time, and robust ventilation for safe time—to mitigate its risks effectively.

3.6. Effect of obstacles on danger time and safe time

This section investigates the impact of obstacles on both danger time and safe time. Fig. 9 shows two models: Model 1 represents an empty indoor environment, while Model 2 includes obstacles such as desks and a commode. For both models, the inlet velocity is set to 0.5 m/s. The inlet concentration for the danger time scenario is 100 mg/m³, whereas the initial concentration for the safe time scenario is 750 mg/m³.

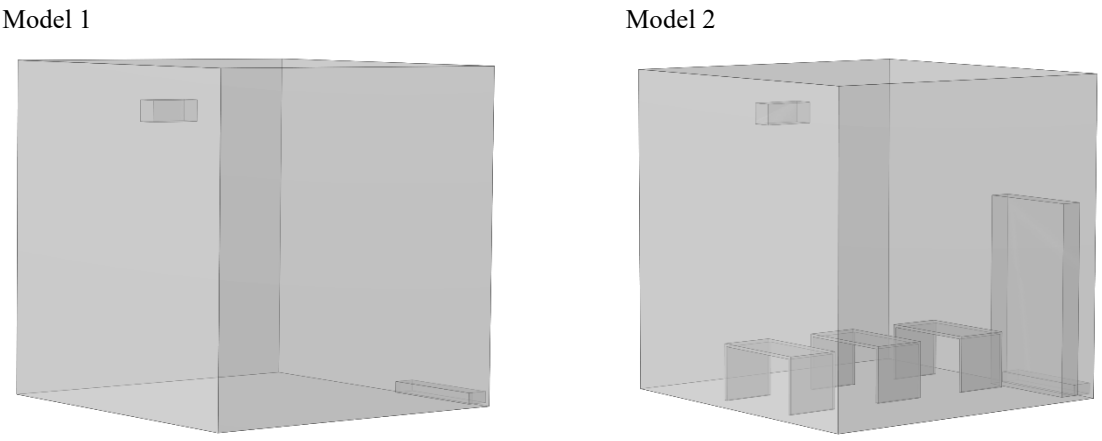

Fig. 9. Indoor environment models: Model 1 without obstacles, Model 2 with obstacles (desk and commode)

Table 2 presents the corresponding danger and safe times for each model. The results clearly indicate that both danger time and safe time increase when obstacles are present in the room. This outcome is attributed to fluid dynamic behavior; the inclusion of obstacles increases resistance to airflow, which slows the dispersion and removal of gas. Consequently, the gas remains in the room for a longer period, leading to an increase in both the time required to reach a dangerous concentration and the time needed to reduce the concentration to safe levels. Additionally, the altered airflow patterns caused by the obstacles reduce the efficiency of gas ventilation.

Table 2. Danger time and safe time for the Model 1 and Model 2

Model	Danger time	Safe time
Model 1	0.35	34.5
Model 2	0.54	49.6

4. Conclusions

This study conducted an investigation into the distribution, danger time, and safe time of VX gas within an indoor environment utilizing a transient three-dimensional CFD approach. The CFD model employed included conservation equations of continuity, momentum, turbulence, and mass transfer.

To assess danger time, air containing the toxic VX gas was introduced into the indoor environment, and the duration required for the concentration of VX to reach 10 mg/m³, the designated danger threshold, was calculated. Conversely, in the safe time scenario, fresh air was introduced to reduce the indoor concentration of VX gas below 0.1 mg/m³, the established safe threshold, and the time necessary to achieve this reduction was determined.

Prior to evaluating danger and safe times, the CFD model underwent a rigorous verification and validation process. Following this, the analysis focused on the distribution of VX concentration and velocity. The study subsequently assessed the influence of inlet velocity and inflow concentration on danger time, as well as the impact of inlet velocity and initial VX concentration on safe time.

The principal conclusions derived from this study are as follows:

- VX gas concentration is notably higher in proximity to walls compared to the center of the indoor space, indicating that areas adjacent to the walls present an increased hazard.
- An increase in inlet velocity from 0.5 m/s to 1.5 m/s results in a decrease in safe time from 40.8 minutes to 13.4 minutes, reflecting a reduction of 67.1%. This underscores the substantial effect of inlet velocity on the rate of gas removal and the overall safety of the indoor environment.
- An increase in initial VX concentration from 500 mg/m³ to 1000 mg/m³ corresponds to an increase in safe time by 9.3%. This finding demonstrates that higher initial concentrations lead to extend safe times due to prolonged gas removal processes.
- When the inlet velocity rises from 0.5 m/s to 1.5 m/s, danger time significantly decreases from 0.4 minutes to 0.13 minutes, representing a reduction of 67.5%. This highlights the critical importance of air velocity in affecting the dispersion and impacts of hazardous gases in confined spaces.
- Additionally, as inflow concentration increases from 100 mg/m³ to 300 mg/m³, danger time decreases from 0.2 minutes to 0.06 minutes, reflecting a reduction of 70%. This observation emphasizes the significance of inflow concentration as a crucial factor influencing gas dispersion and the associated risks in enclosed environments.

Ethical statement

This study is conducted solely for scientific and safety purposes, aiming to enhance understanding of hazardous gas dispersion for risk mitigation and emergency response. The findings are intended to support protective measures and do not promote or facilitate the misuse of such information for harmful purposes.

References

[1] Mukhopadhyay, S., Schoenitz, M., Dreizin, E.L., 2021, Vapor-phase decomposition of dimethyl methylphosphonate (DMMP), a sarin surrogate, in presence of metal oxides, Defence Technology, 17, 1095-1114. https://doi.org/10.1016/j.dt.2020.08.010

[2] Lee, E.C., 2003, Clinical manifestations of sarin nerve gas exposure, Jama, 290, 659-662. https://doi.org/10.1001/jama.290.5.659

[3] Kye, Y.-S., Chung, W.-Y., Kim, Y.-J., 2012, A study on the decomposition of DFP using Cu (II)-chitosan complex, Journal of the Korea Institute of Military Science and Technology, 15, 699-704. https://doi.org/10.9766/kimst.2012.15.5.699

[4] Aldahhak, H., Powroźnik, P., Pander, P., Jakubik, W., Dias, F.B., Schmidt, W.G., Gerstmann, U., Krzywiecki, M., 2020, Toward efficient toxic-gas detectors: Exploring molecular interactions of sarin and dimethyl methylphosphonate with metal-centered phthalocyanine structures, The Journal of Physical Chemistry C, 124, 6090-6102. https://doi.org/10.1021/acs.jpcc.9b11116

[5] Ma, L., Chen, B., Qiu, S., Li, Z., Qiu, X., 2017, Agent-based modeling of emergency evacuation in a railway station square under sarin terrorist attack, International Journal of Modeling, Simulation, and Scientific Computing, 8, 1750022. https://doi.org/10.4103/atr.atr4019

[6] Davis, E.D., Gordon, W.O., Wilmsmeyer, A.R., Troya, D., Morris, J.R., 2014, Chemical warfare agent surface adsorption: hydrogen bonding of sarin and soman to amorphous silica, The Journal of Physical Chemistry Letters, 5, 1393–1399. https://doi.org/10.1021/jz500375h

[7] Balow, R.B., McEntee, M., Schweigert, I.V., Jeon, S., Peterson, G.W., Pehrsson, P., 2021, Battling chemical weapons with zirconium hydroxide nanoparticle sorbent: impact of environmental contaminants on sarin sequestration and decomposition, Langmuir, 37, 6923–6934. https://doi.org/10.1021/acs.langmuir.1c00380

[8] Singer, B.C., Hodgson, A.T., Destaillats, H., Hotchi, T., Revzan, K.L., Sextro, R.G., 2005, Indoor sorption of surrogates for sarin and related nerve agents, Environmental Science & Technology, 39, 3203–3214. https://doi.org/10.1021/es049144u

[9] Li, T., Leonard, M., Tsyshevsky, R., McEntee, M., Karwacki, C., Durke, E.M., Kuklja, M.M., Rodriguez, E.E., 2023, High reactivity of mesoporous CeO_2 to dissociate chemical warfare agent sarin, Materials Chemistry Frontiers, 7, 1855–1866. https://doi.org/10.1039/D2QM01253G

[10] Tsyshevsky, R., Head, A.R., Trotochaud, L., Bluhm, H., Kuklja, M.M., 2020, Mechanisms of degradation of toxic nerve agents: quantum-chemical insight into interactions of sarin and soman with molybdenum dioxide, Surface Science, 700, 121639. https://doi.org/10.1016/j.susc.2020.121639

[11] Chauhan, N., Chauhan, R., 2015, Active-passive measurements and CFD based modelling for indoor radon dispersion study, Journal of Environmental Radioactivity, 144, 57–61. https://doi.org/10.1016/j.jenvrad.2015.03.009

[12] Zhou, W., Iida, T., Moriizumi, J., Aoyagi, T., Takahashi, I., 2001, Simulation of the concentrations and distributions of indoor radon and thoron, Radiation Protection Dosimetry, 93, 357–367. https://doi.org/10.1093/oxfordjournals.rpd.a006448

[13] Hosseini, M., Madani, H., Shahriar, K., 2022, CFD-based modeling of sarin gas dispersion in a subway station – A hypothetical scenario, Journal of Mining and Environment, 13, 235–251. https://doi.org/10.22044/jme.2022.11604.2150

[14] Parkash, R., Chauhan, N., Chauhan, R., 2024, Application of CFD modeling for indoor radon and thoron dispersion study: A review, Journal of Environmental Radioactivity, 272, 107368. https://doi.org/10.1016/j.jenvrad.2023.107368

[15] Faugier, L., Marinus, B.G., Bosschaerts, W., Laboureur, D., Limam, K., 2023, CFD model for airflow in a subway station compared to on-site measurements: The challenges of as-built environment, Tunnelling and Underground Space Technology, 140, 105248. https://doi.org/10.1016/j.tust.2023.105248

[16] Lin, X., Fu, Y., Peng, D.Z., Liu, C.-H., Chu, M., Chen, Z., Yang, F., Tim, K., Li, C.Y., Feng, X., 2024, CFD- and BPNN-based investigation and prediction of air pollutant dispersion in urban environment, Sustainable Cities and Society, 100, 105029. https://doi.org/10.1016/j.scs.2023.105029

[17] Yang, L., Ye, M., 2014, CFD simulation research on residential indoor air quality, Science of the Total Environment, 472, 1137–1144. https://doi.org/10.1016/j.scitotenv.2013.11.118

[18] Widiatmojo, A., Sasaki, K., Widodo, N.P., Sugai, Y., Sahzabi, A.Y., Nguele, R., 2016, Predicting gas dispersion in large scale underground ventilation: A particle tracking approach, Building and Environment, 95, 171–181. https://doi.org/10.1016/j.buildenv.2015.07.025

[19] Dolezal, O., Tomaskova, H., 2020, An agent-based simulation to minimize losses during a terrorist attack, Applied Sciences, 10, 3213. https://doi.org/10.3390/app10093213

[20] Siddiqui, M., Jayanti, S., Swaminathan, T., 2012, CFD analysis of dense gas dispersion in indoor environment for risk assessment and risk mitigation, Journal of Hazardous Materials, 209, 177–185. https://doi.org/10.1016/j.jhazmat.2012.01.007

[21] Chunwen, X., Shuquan, Y., Jianfeng, T., Mengjie, S., 2024, Design and practice of indoor gas leak diffusion simulation experiment based on CFD, Experimental Technology and Management, 41, 119–126. https://doi.org/10.16791/j.cnki.sjg.2024.12.016

[22] Li, L., He, Y., Chen, W., Ji, Y., Fung, J.C., Lau, A.K., 2024, An integrated experimental and CFD analysis of ceiling-fan-integrated air conditioning system: Indoor air quality and air velocity, Building and Environment, 258, 111633. https://doi.org/10.1016/j.buildenv.2024.111633

[23] Wang, S., Zheng, X., Ng, S.T., Bao, Z., 2024, An innovative three-dimensional computational fluid dynamics-iterative ensemble Kalman filter model for the prediction of heavy gas leakage and dispersion in enclosed workplaces: Case study for hydrogen sulfide leakage, Physics of Fluids, 36. https://doi.org/10.1063/5.0216440

[24] Eckstein, A., Gilliard, J., Lee, A., Banko, A., Fobar, D., 2024, Contaminant dispersion: Modeling indoor and outdoor airflow through a ventilated building, ASME International Mechanical Engineering Congress and Exposition, American Society of Mechanical Engineers, V008T010A046. https://doi.org/10.1115/imece2024-145306

[25] De Crescenzo, C., Sabbarese, S., Ciampa, R., Capece, G., Migliaccio, A., Karatza, D., Chianese, S., Musmarra, D., 2021, Simulation of methane mass transfer in a bubble column incipient turbulent regime using COMSOL Multiphysics®, Chemical Engineering Transactions, 86, 1183–1188. https://doi.org/10.1016/j.nbt.2022.04.004

[26] Ganguli, A., Kenig, E., 2011, A CFD-based approach to the interfacial mass transfer at free gas–liquid interfaces, Chemical Engineering Science, 66, 3301–3308. https://doi.org/10.1016/j.ces.2011.01.055

[27] Ma, R., Castro-Dominguez, B., Dixon, A.G., Ma, Y.H., 2018, CFD study of heat and mass transfer in ethanol steam reforming in a catalytic membrane reactor, International Journal of Hydrogen Energy, 43, 7662–7674. https://doi.org/10.1016/j.ijhydene.2017.08.173

[28] Agarwal, T.K., Sahoo, B., Joshi, M., Mishra, R., Meisenberg, O., Tschiersch, J., Sapra, B., 2019, CFD simulations to study the effect of ventilation rate on 220Rn concentration distribution in a test house, Radiation Physics and Chemistry, 162, 82–89. https://doi.org/10.1016/j.radphyschem.2019.04.018